The 2009 IEEE/RSJ International Conference on
Intelligent Robots and Systems
October 11-15, 2009 St. Louis, USA

Fast Experimental Estimation of Drag Coefficients of Arbitrary Structures

G. Kósa, R. Hoever, D. Szczerba, G. Székely, M. Harders

Abstract— **We present a setup for simple and fast experimental estimation of drag coefficients. Our system can accurately determine the parameters of fluid-object interaction for complicated geometry and boundary conditions in the realm of classical Stokes equations. Obtained results are compared with theoretical and numerical solutions. Good agreement with those references is achieved in both cases. An advantage of our method is the prompt and easy parameter retrieval that still maintains appropriate accuracy. Comparable detailed numerical estimations run on the order of hours or days.**

I. INTRODUCTION

In our current research we examine the interaction between objects and fluidic environments on micro/nano-scale. Knowledge about this relationship is for instance essential for the development of miniature swimming robots [1]. In addition, determination of the parameters of an underlying object-fluid interaction model will also be helpful for interactive manipulation of micro/nano-structures, for instance to provide appropriate forces in a visuo-haptic tele-manipulation environment [2].

Direct observation of the motion of micro/nano-devices in a fluidic environment is complicated. Using a microscope enables recording only in the focal plane in a limited area. Also, it is hard to determine boundary conditions, for instance contacts with other structures.

One possibiliy to analyze the object-fluid interaction is numerical simulation [3], [4], however, the computations are time-consuming and determination of boundary conditions is not straight-forward. Another option is building of upscaled models of the micro/nano-devices and experimenting in highly viscous fluids. Until now, such experimental methods only concentrated on determination of propulsive forces due to flagellar swimming motions [5], [6].

Therefore, we have developed a setup for simple and fast experimental estimation of drag coefficients. The apparatus allows retrieving flow parameters of arbitrary structures subject to complex fluid-solid interaction. The advantage of our method is the fast parameter retrieval process, especially for low Reynolds number flows, while maintaining overall accuracy. The described approach is appropriate as long as the phenomena can be captured completely by classical Stokes equations.

This work was supported by the Immersence project EU IST-2006-27141.

G. Kósa, R. Hoever, G. Székely, M. Harders are with the Computer Vision Laboratory, Department of Information Technology and Electrical Engineering, ETH Zurich, 8092 Zurich, Switzerland (e-mail: gkosa@vision.ee.ethz.ch, phone: 41-44-6327689; fax: 41-44-6321199)

D. Szczerba is with the IT'IS Foundation, 8092 Zurich, Switzerland.

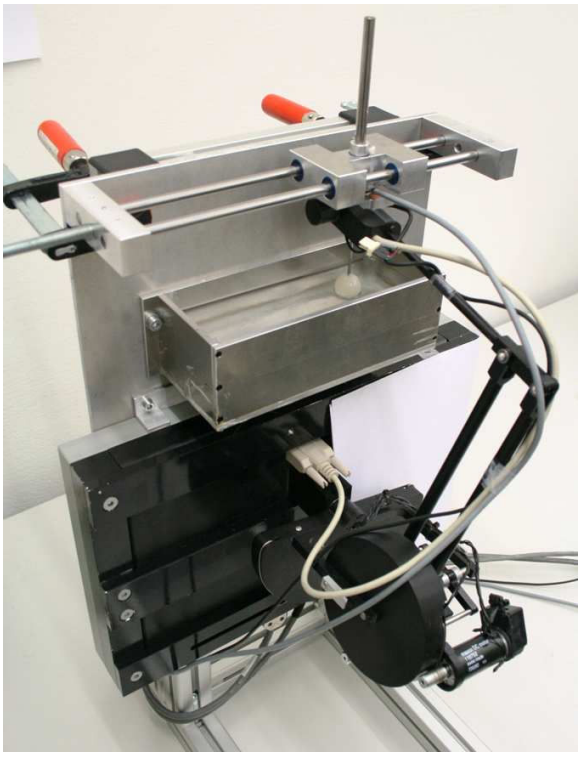

(a) Picture of setup with (top to bottom) sliding mechanism, probe with force and acceleration sensor, mounted test object, vessel with fluid, PHANToM device.

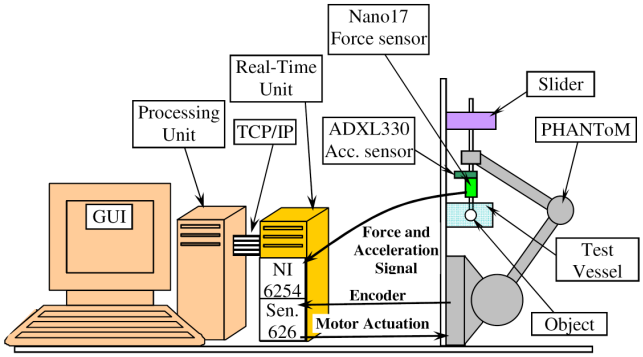

(b) Schematic drawing of system components.

Fig. 1. Setup for experimental parameter estimation.

The underlying principle is to record forces and velocities during movement of a target structure within a fluidic environment. A specialized recording apparatus has been integrated for the acquisition process. Based on the acquired data, the drag coefficients are determined. In this paper

we focus on the estimation of parameters in low Reynolds number flows, i.e. Stokes flow. The underlying equations describing these environments and the derivation of a reduced formulation are given in the Appendix.

In the context of our experiments, the most important part of the full interaction equation (see e.g. [8]) is the relation between the drag force $\mathbf{f}$ and the linear velocity $\mathbf{v}$ given by

$$\mathbf{f} = \mu r \mathbf{K}(p, P)\mathbf{v} \tag{1}$$

where μ is the absolute viscosity, p the external pressure function, and P are geometrical parameters of the object. The dimensionless second order drag coefficient tensor $\mathbf{K}(p, P)$ is a full symmetric matrix, which can be simplified by taking symmetries of the interacting object into account. We have carried out experiments with the setup focusing on two types of test objects – spheres and helices. In case of objects with two symmetry planes, such as a sphere, the drag tensor $\mathbf{K}(p, P)$ has only one term, while in case of a helix it has two.

After determining the parameters, the obtained experimental results are compared with theoretical and numerical solutions. We show that a good agreement with these numbers can be obtained.

In the following, the setup used for acquiring the drag coefficients is described in Section II. Thereafter, experiments with spherical test objects are outlined in Section III. This is followed by the second study focusing on helices in Section IV. We conclude with a summary of the presented work and an outlook to future activities.

II. EXPERIMENTAL SETUP

A hardware framework, initially developed for data-driven haptic rendering [7], has been adapted to account for fluid-object interaction. A picture of the setup and a schematic drawing of the system components is shown in Figure 1.

A PHANToM Desktop 1.5/3DOF (Sensable) is used as the main component of the force recording system. A Nano-17 6-DOF force sensor (ATI, Industrial Automation) and an ADXL330 3-DOF acceleration sensor (Analog Devices) is mounted to the stylus of the PHANToM, which serves as a probing rod. The range of the force sensor is $\pm 25\,N$ with a resolution of $1.6\,mN$ and a noise level of $0.02\,N$. The range of the acceleration sensor is $\pm 30\,m/s^2$ with a resolution of $0.9\,mm/s^2$ and a noise level of $0.1\,m/s^2$. The motion of the probing tool is limited to one DOF by a sliding mechanism. A vessel with dimensions $200\times80\times50$ mm^3 is installed under the slider and filled with a testing fluid. In our experiments we used Dow Corning 200 12500 cSt Silicon Oil with an absolute viscosity of $\mu = 12.125$ Pas and specific gravity of $\rho = 970$ kg/m^3.

The rigid sample object is attached to the sensing tool by an M2 screw rod (Figure 2). The object is fully submerged into the testing fluid (i.e. the silicone oil), while the depth of immersion is held constant, assuring well defined boundary conditions during the experiment. Thereafter, the probe is moved along the slider at different velocities by a user. The size of the test objects should be small in relation to the vessel in order to minimize any effects of the vessel wall on the measurements. The interaction is recorded by the motion and force sensors simultaneously at a sampling frequency of 1 kHz.

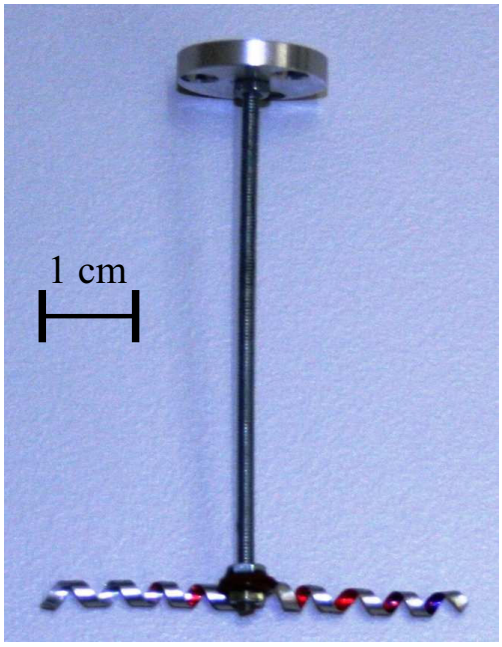

Fig. 2. Helix II mounted for lateral drag test.

The drag coefficient is estimated by computing the ratio between the force and the velocity during the interaction. The force exerted by the fluid is measured directly by the attached sensor. The linear velocity of the object is estimated based on the PHANToM encoder readings and the ADXL330 acceleration sensor output. Both signals are fused by an extended Kalman filter. If the encoder values were directly used in a numerical derivation, the velocity estimate would be too noisy to obtain reasonable results. The filter approach avoids any explicit derivation and allows to estimate the current velocity based on two independent quantities, namely position and acceleration. The method provides a consistent estimate of the current pose, velocity, and acceleration of the tool. A linear interpolation is then fitted to these force-velocity samples. The slope of the fit finally gives the respective drag coefficient in the drag tensor.

III. EXPERIMENT 1 – SPHERE

In the first experiment we focus on objects with simple geometries and boundary conditions. The main reason for this is the possibility to determine an analytical solution for the tensor in Equation 1, thus providing an accurate ground truth for the evaluation. This is possible due to the linearity of the Stokes equation which governs low Reynolds number flows [8].

The analytical derivation of the drag force of a sphere has been described already in 1851 by Stokes. For a sphere moving in an infinite media this is known as Stokes' law. Later

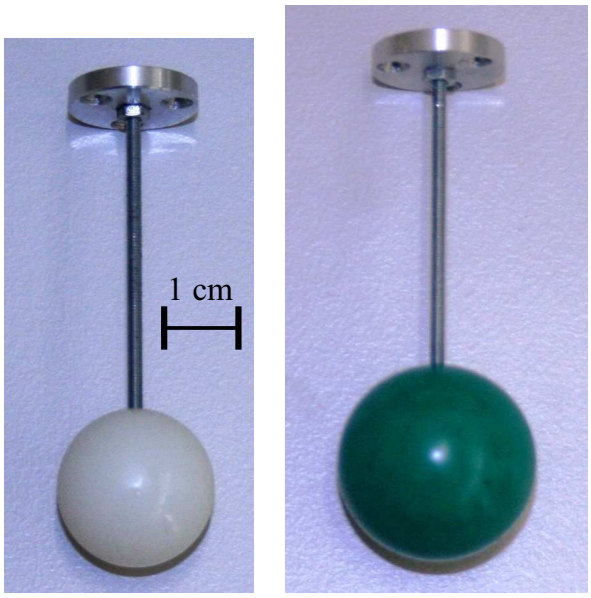

(a) Sphere I. (b) Sphere II.

Fig. 3. Sphere-shaped test objects.

work expanded Stokes' law to other boundary conditions, for instance to a sphere in translation near a wall [9], which will be used in our case.

The overall drag force is a superposition of the drag force of the sphere moving parallel to the wall located at the bottom of the test vessel and the transverse drag force of the testing rod. Thus, according to the relations given in [9] and [10], the analytical solution for the drag coefficient has the form

$$K_{11} = K_{22} = 6\pi\beta + \frac{4\pi L}{R_s\left(\ln(L/R_r) + 0.19314\right)}. \quad (2)$$

Here, the first term is based on the standard Stokes' law, extended with a correction ratio β that models the increase of the sphere's drag due to its proximity to a wall (see [9] for details). The second term corresponds to the transverse drag caused by the rod. The characteristic dimensions of the objects are the radius of the sphere R_s, the radius of the rod R_r, and the length L of the submerged part of the rod.

Two spheres were used in the experiments – Sphere I (⌀20 mm) and Sphere II (⌀25 mm), respectively (Figure 3). In the experiments the level of the Silicon oil inside the vessel was 5 cm. Sphere I was located 8 mm and Sphere II 5 mm from the bottom, resulting in correction ratios of $\beta = 1.422$ and $\beta = 1.533$, respectively. For each of the spheres three experiments were performed.

Figure 4(a) shows a typical force-velocity graph obtained during an experiment with Sphere I. A comparison of recorded data and estimates given by Equation 1, when using the estimated drag coefficient, is depicted in Figure 4(b). It can be seen that Equation 1 is an appropriate model for the examined object-fluid interaction.

The obtained drag coefficients were then compared to the theoretical values. The properties of the liquid were

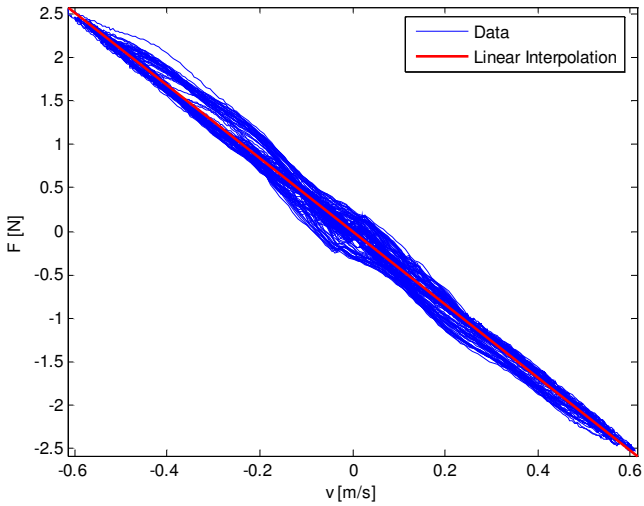

(a) Relation of force and velocity, recorded (blue) and linear interpolation (red).

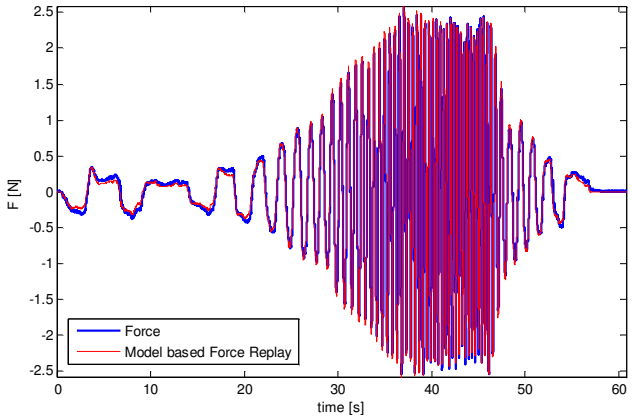

(b) Recorded force over time (blue) and force synthesized based on retrieved drag coefficient (red).

Fig. 4. Data retrieved from the experiment.

assumed as given by the manufacturer's technical data. It was not necessary to match the viscosity to the specific experimental conditions (i.e. temperature, humidity, etc.), thus drag coefficients have not been normalized. Note that the absolute drag coefficient is given as

$$\tilde{\mathbf{K}} = \mu R_s \mathbf{K}, \quad (3)$$

where $\tilde{\mathbf{K}}$ is the normalized resistance tensor and μ the absolute viscosity.

Table I summarizes the results of the experiments. The average drag coefficients of Sphere I and II are -4.206 ± 0.0036 [Ns/m] and -5.298 ± 0.096 [Ns/m], respectively. The maximal error between the experiments and the theory is 0.77%. The coefficient of variance (i.e. the relative standard deviation) is 1.81%. Thus, an excellent agreement between our results and the analytical solution could be obtained.

TABLE I

EXPERIMENTAL RESULTS OF SPHERICAL TEST OBJECTS AND COMPARISON TO ANALYTICAL SOLUTIONS.

Test object	Exp.	$\tilde{K}_{11}$ [Ns/m]	Difference from average [%]
Sphere I	1	-4.209	-0.07
	2	-4.202	0.095
	3	-4.207	-0.023
Theoretical solution		-4.223	-0.4
Sphere II	1	-5.19	2.0
	2	-5.33	-0.6
	3	-5.374	-1.43
Theoretical solution		-5.257	0.77

TABLE II

GEOMETRICAL DETAILS OF HELICAL TEST OBJECTS.

Object	Geometries
Helix I	Diameter: 2.8 mm Length: 55 mm Strip width: 6 mm Strip thickness: 0.15 mm Pitch angle: 45°
Helix II	Diameter: 2.8 mm Length: 40 mm Strip width: 1.7 mm Strip thickness: 0.15 mm Pitch angle: 45°
Nano-Helix [1]	Diameter: 2.8 μm Length: 40 μm Strip width: 2 μm Strip thickness: 50 nm Pitch angle: 45°

IV. EXPERIMENT 2 – HELIX

In order to assess the performance of our approach in case of more complex geometries, an additional experiment was carried out. Inspired by the propulsion systems for swimming micro-robots discussed in [1], we examined helical test objects. Two different helices, Helix I and II, respectively, were examined. The dimensions of these test objects are given in Table II. Moreover, also the values of the nano-helix described in [1] are provided. The dimensions of Helix II were chosen to be similar to those of the nano-helix for later comparison. Figure 5 shows the different helical objects.

A helical object exhibits helical symmetry, i.e. one axis of symmetry, thus the object-fluid interaction is determined by the tensor

$$\tilde{\mathbf{K}} = \begin{bmatrix} \tilde{K}_{11} & 0 & 0 \\ 0 & \tilde{K}_{11} & 0 \\ 0 & 0 & \tilde{K}_{33} \end{bmatrix}. \quad (4)$$

Similar to the previous experiment, the mounted test objects were moved through the liquid and data acquired via the sensors. In order to find the drag coefficients of the helix without the connecting rod, we carried out additional experiments with the rod alone. The obtained drag of the rod was then subtracted from that of the whole structure. The results again were compared to a ground truth.

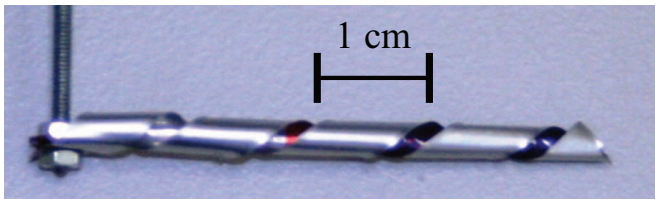

(a) Helix I.

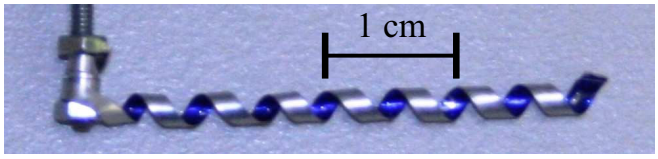

(b) Helix II.

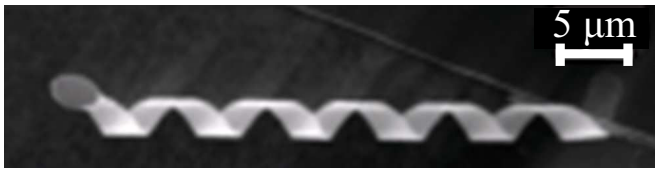

(c) Nano-Helix (with permission from [1]).

Fig. 5. Helical test objects.

Unfortunately, finding an analytical solution for the drag coefficients of helical structures is rather difficult. Therefore, we relied on numerical simulations for obtaining those values. Assessment of flow conditions using numerical techniques is a frequent practice in micro-mechanical design involving arbitrary geometries. The helix geometry and the containing vessel were modeled in a CAD application and subsequently covered by an adaptively fitted unstructured mesh of up to 600,000 second order elements. For the discretization of the equations the standard Bubnov-Galerkin method was applied [11]. This resulted in a system of linear equations that was subsequently solved with a high-performance library for sparse asymmetric linear systems, PARDISO [12], [13]. The typical computation times of a solution were 1-4 h on an octacore shared memory PC, mainly dependent on the mesh resolution. The method proved capable of delivering detailed predictions on the flow situation, including secondary spinning flows in directions other than the dominating movement. Figure 6 provides illustrations of the numerical computation.

Tables III and IV summarize the results of the helix experiments. Only average values are provided that result from five different experiments. For Helix I only $\tilde{K}_{11}$ was determined in the numerical simulation, while for Helix II both coefficients were retrieved. Further, Reynolds numbers are given, showing that the experiments are in the domain of Stokes flow.

Moreover, since one of our motivations was the characterization of drag parameters of micro- or nano-structures, we also examined if our results compare well to data obtained for real nano-helices. For this comparison, we assume that

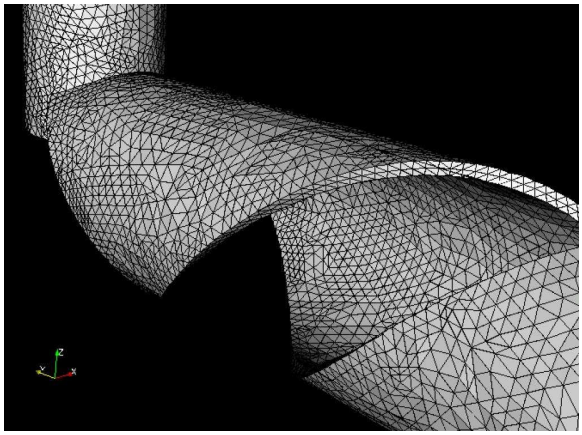

(a) Tetrahedral mesh used in numerical simulation.

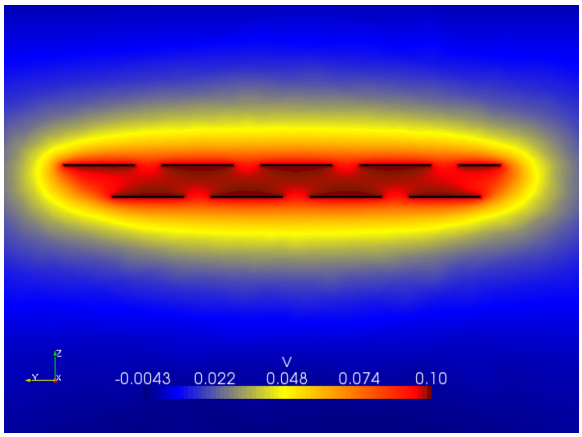

(b) Velocity in y-direction viewed in y-z plane.

Fig. 6. Numerical simulation of flow around helix.

the non-dimensional drag coefficient matrix $\mathbf{K}$ is the same for Helix II and the nano-helix. Based on this assumption one can calculate the drag of the nano-helix as

$$\begin{aligned} \tilde{K}_{11}^{NH} &= \frac{\mu^{NH}}{\mu^{HelixII}} \frac{R^{NH}}{R^{HelixII}} \tilde{K}_{11}^{HelixII} \\ &= 8.247 \cdot 10^{-8} \tilde{K}_{11}^{HelixII} \end{aligned} \quad (5)$$

where $\mu^{NH} = 10^{-3}$ Pa·s and $\mu^{HelixII} = 12.125$ Pa·s are the viscosities, and $R^{NH}, R^{HelixII}$ the radii of the nano-helix and Helix II, respectively.

Using Equation 5 we calculate for the nano-helix $\tilde{K}_{11} = -7.08 \cdot 10^{-8}$ [Ns/m]. This compares well to the experimentally obtained coefficient available in related work $\tilde{K}_{11} = -9.2 \cdot 10^{-8}$ [Ns/m].

The simulation results revealed a good agreement between the experimental and the numerical methods with a maximal error of 9% and maximal coefficient of variance of 5.8%.

When considering these results it has to be taken into account that there are slight differences between the real helices and the modeled, digital ones. The former show some variation from the perfect shape. Moreover, the numerical simulation only provides an approximation of an exact solution. Nevertheless, it has to be considered that a single numerical run consumes large computational resources and requires substantially more time (1-4 h) than a simple experiment using our setup that can be finished in 5 minutes.

TABLE III

EXPERIMENTAL RESULTS OF HELIX I AND COMPARISON TO NUMERICAL SOLUTIONS.

Experiment		$\tilde{K}_{ii}$ [Ns/m]	Re number
Helix + Rod	$\tilde{K}_{11}$	-2.723 ± 0.07	0.057 ± 0.0057
	$\tilde{K}_{22}$	-3.66 ± 0.006	0.0058 ± 6.7·10^{-4}
Rod	$\tilde{K}_{11}$	-1.489 ± 0.03	0.071 ± 0.016
	$\tilde{K}_{22}$	-1.04 ± 0.024	-
Helix	$\tilde{K}_{11}$	-1.233 ± 0.1	-
	$\tilde{K}_{22}$	-2.62 ± 0.03	-
Numerical result		$\tilde{K}_{ii}$ [Ns/m]	Re number
Helix + Rod	$\tilde{K}_{11}$	-2.57	-
Helix	$\tilde{K}_{11}$	-1.468	-

TABLE IV

EXPERIMENTAL RESULTS OF HELIX II AND COMPARISON TO NUMERICAL SOLUTIONS.

Experiment		$\tilde{K}_{ii}$ [Ns/m]	Re number
Helix + Rod	$\tilde{K}_{11}$	-2.233 ± 0.046	0.021 ± 0.0068
	$\tilde{K}_{22}$	-3.628 ± 0.017	0.0038 ± 4.3·10^{-4}
Rod	$\tilde{K}_{11}$	-1.374 ± 0.0126	0.026 ± 0.0093
Helix	$\tilde{K}_{11}$	-0.859 ± 0.06	-
	$\tilde{K}_{22}$	-2.254 ± 0.03	-
Numerical result		$\tilde{K}_{ii}$ [Ns/m]	Re number
Helix + Rod	$\tilde{K}_{11}$	-2.44	-
	$\tilde{K}_{22}$	-3.72	-

V. CONCLUSIONS AND FUTURE WORKS

We have presented an experimental framework that enables retrieval of parameters of fluid-object interaction. The setup can measure accurately the drag coefficient of objects with complicated geometry and boundary conditions. Our system is valid for phenomena that can be described completely by classical Stokes equations. Systems with more complex effects such as adsorption or surface tension, however, cannot be fully captured with the current technique. Obtained measurements were compared with theoretical and numerical ground truths. In both experiments good agreement with those references was obtained.

In the future we intend to expand the interaction measurements to find the complementary drag coefficient tensors $(\mathbf{\Omega}, \mathbf{C})$ and address intermediate Reynolds number fluid-object interactions. These parameters will be used for the development of swimming theories for micro/nano-robots. Moreover, the framework will also aid us in retrieving haptic models for micro-robots, for instance in the medical domain. Finally, a possible application of our setup is in the context of tele-manipulation of nano-robots, where it is hard to measure interaction forces directly.

VI. ACKNOWLEDGMENTS

This work was supported by the Immersence project EU IST-2006-27141.

APPENDIX

The interaction of a rigid object with a liquid can be described using the force and torque vectors $\mathbf{f}$ and $\boldsymbol{\tau}$, respectively.

$$\begin{aligned} \mathbf{f} &= (\rho + \rho_m)\mathbf{g}_1(\mathbf{x}, \dot{\mathbf{x}}, p, P)\ddot{\mathbf{x}} + \mu\mathbf{g}_2(\mathbf{x}, \dot{\mathbf{x}}, p, P)\dot{\mathbf{x}} \\ \boldsymbol{\tau} &= (\rho + \rho_m)\mathbf{h}_1(\mathbf{x}, \dot{\mathbf{x}}, p, P)\ddot{\mathbf{x}} + \mu\mathbf{h}_2(\mathbf{x}, \dot{\mathbf{x}}, p, P)\dot{\mathbf{x}} \quad (6) \end{aligned}$$

where $\mathbf{x} = [x, y, z, \phi, \theta, \psi]^T$ denotes the linear and angular position of the object in the liquid, $\dot{\mathbf{x}}$ is the velocity and $\ddot{\mathbf{x}}$ is the acceleration vector, describing both linear and angular components. $\mathbf{g}_i, \mathbf{h}_i$ are second order tensors consisting of non-linear shape functions depending on position, velocity, the external pressure function p, and geometrical parameters P of the object. ρ is the density of the liquid, ρ_m is the added mass, and μ is the absolute viscosity of the liquid.

Usually, the material parameters ρ and μ, as well as the geometry P of the object are known. Hence, one has to find the pressure function p, the shape tensors $\mathbf{g}_i, \mathbf{h}_i$, and the added mass ρ_m.

For simple cases, these unknowns can be determined analytically. More involved scenarios require numerical approaches using CFD software or parameter estimation via experimentation.

In the application areas we are interested in (i.e. microfluidics), flow is characterized by low Reynolds numbers and thus inertial components of the interaction can be neglected.

$$\begin{aligned} \mathbf{f} &= \mu\mathbf{g}_2(\mathbf{x}, \dot{\mathbf{x}}, p, P)\dot{\mathbf{x}} \\ \boldsymbol{\tau} &= \mu\mathbf{h}_2(\mathbf{x}, \dot{\mathbf{x}}, p, P)\dot{\mathbf{x}} \quad (7) \end{aligned}$$

Considering self induced propulsion and position independent drag, one can define the following linear interaction:

$$\begin{bmatrix} \mathbf{f} \\ \boldsymbol{\tau} \end{bmatrix} = \mu r \begin{bmatrix} \mathbf{K}(p, P) & \mathbf{C}(p, P) \\ \mathbf{C}(p, P)^T & \boldsymbol{\Omega}(p, P) \end{bmatrix} \begin{bmatrix} \mathbf{v} \\ \boldsymbol{\omega} \end{bmatrix} \quad (8)$$

where r is the characteristic dimension of the structure of interest (e.g. diameter of a nano-helix) and $\mathbf{K}(p, P)$ is a dimensionless second order drag coefficient tensor that defines the relation between the linear velocity $\mathbf{v}$ and the force $\mathbf{f}$. $\boldsymbol{\Omega}(p, P)$ relates the angular velocity $\boldsymbol{\omega}$ to the moment $\boldsymbol{\tau}$. $\mathbf{C}(p, P)$ converts angular velocity into force, and its transpose linear velocity into torque.

For our work, the most important part of the full interaction model is the relation between the drag force $\mathbf{f}$ and the linear velocity $\mathbf{v}$, described by Equation 1.

REFERENCES

[1] J. J. Abbott, K. E. Peyer, L. X. Dong and B. J. Nelson, "How Should Microrobots Swim?" Robotics Research: Results of the 13th International Symposium ISRR, London: Springer-Verlag, 2008.

[2] D.-H. Kim, K. Kim, K.-Y. Kim and S.-M. Cha, "Dexterous Teleoperation for Micro Parts Handling based on Haptic/Visual Interface", Proceedings of the IEEE International Symposium on Micromechatronics and Human Science, pp. 211-217, 2001.

[3] R. Tyson, C. E. Jordan and J. Hebert, Interactions between comoving magnetic microswimmers, Physical Review E, vol. 77, pp. 041910, 2008.

[4] R. Dillon, L. Fauci and D. Gaver III, A Microscale Model of Bacterial Swimming, Chemotaxis and Substrate Transport, J. theor. Biol., vol. 177, pp. 325-340, 1995.

[5] B. Behkam and M. Sitti, "Design methodology for biomimetic propulsion of miniature swimming robots", J. Dyn. Sys. Meas. Con. Trans. Asme, vol. 128, pp. 36-43, 2006.

[6] T. S. Yu, E. Lauga and A. E. Hosoi, Experimental investigations of elastic tail propulsion at low Reynolds number, Physics of Fluids, vol. 18, pp. 091701, 2006.

[7] R. Hoever, M. Harders and G. Szekely, "Data-driven haptic rendering of visco-elastic effects," in Proc. of IEEE Haptic Symposium, Reno, 2008, pp. 201-208.

[8] J. Happel and H. Brenner, Low Reynolds number hydrodynamics, Boston: Springer-Verlag, 1983, ch. 4.

[9] A. Ambari, B. Gauthier Manuel, and E. Guyon., "Effect of a plane wall on a sphere moving parallel to it", J. Physique Lettres, vol. 44, pp. L143-L146, February 1983.

[10] R.G. Cox, "The motion of long slender bodies in a viscous fluid Part 1. General theory," J. Fluid Mech., vol. 44, pp. 791-810, April 1970.

[11] O. Zienkiewicz and R. Taylor, The Finite Element Method, Oxford: Butterworth-Heinemann, 2000.

[12] O. Schenk and K. Gaertner, "Solving Unsymmetric Sparse Systems of Linear Equations with PARDISO", Future Gener. Comp.r Sy., vol. 20, pp. 475-487, April 2004.

[13] O. Schenk and K. Gaertner, "On fast factorization pivoting methods for sparse symmetric indefinite systems", Electron. T. on Numer. Ana., vol. 23, pp. 158-179, 2006.